https://doi.org/10.1016/j.tws.2022.110325

Seismic Design and Parametric Study of Steel Modular Frames with Distributed Seismic Resistance

Chen Wang[1], Tak-Ming Chan[1, *]

[1]Dept. of Civil and Environmental Engineering, The Hong Kong Polytechnic Univ., Hung Hom, Hong Kong.

[*] Email: tak-ming.chan@polyu.edu.hk

Abstract

Structures in modular buildings typically have some unique characteristics as compared with conventional structures, e.g., discrete connection of modules through inter-module connections, discontinuous floor diaphragms. The behavior of steel modular structures under earthquake excitations has not been fully understood, and no seismic design method specifically tailored for modular building structures is available. Moreover, although various inter-module connections with different rotational connectivity have been proposed, their suitability for seismic application is questionable. In this paper, the distributed seismic design method, which makes use of the lateral resistance inherent in all modules, was proposed for modular buildings with steel frames. A numerical parametric study was conducted on a 9-story prototype building. The effect of three parameters, i.e., the rotational stiffness of inter-module connections, the seismic design force level, and the height-wise distribution of the design base shear, were studied. The results show that the rotational stiffness of inter-module connections has limited impact on the elastic lateral stiffness and the fundamental period of modular steel frames. However, in the inelastic range, the increase in the rotational stiffness will lead to less plastic drift concentration and better collapse prevention performance. Increasing the seismic design force may not result in enhanced collapse prevention performance, as it is also dependent on the height-wise distribution of the design base shear and if significant higher-mode response is involved in the total response of the structure.

Keywords: modular buildings, inter-module connection, rotational stiffness, distributed seismic resistance, soft-story mechanism, higher-mode effect

1 Introduction

The modular construction method, in which the off-site prefabricated modules are transported and assembled on site to form the entire building, brings the benefits of improved site safety, reduced workload on site, better quality control, shorter construction period, and less construction waste [Lawson et al., 2012 & 2014; Kamali & Hewage, 2016; Ferdous et al., 2019]. This construction method has, therefore, been promoted in the construction industry around the world, and it is gaining popularity especially for buildings with *repetitive* architectural and structural layouts, e.g., hotels, hospitals, schools, etc. [Smith, 2010; Deng et al., 2020] Steel is popularly used in the structure of modular buildings owning to its flexibility in architectural design, lightweight, and convenience in assembly as compared to concrete or timber framed modules [Lawson & Ogden, 2005; Gatheeshgar et al., 2021].

Modular buildings with steel structures are constructed through assembly of individual modular units as shown in Fig. 1. Coming along with this construction methods are some unique structural characteristics. Firstly, each module typically consists of floor beams and ceiling beams. As such, two layers of beams (floor beam and ceiling beam) exist at each floor level, as compared to only one layer of beams in conventional buildings. Secondly, modular units are usually connected between corner columns through inter-module connections. Floor diaphragms of modular buildings are therefore discontinuous, while diaphragms at each floor in conventional buildings are continuous. Moreover, although various types of inter-module connections have been proposed [Deng et al., 2018; Chen et al., 2017a & 2017b; Lacey et al., 2019; Dai et al., 2020; He et al., 2021], focus has been mostly on their axial and shear strength, and limited rotational connectivity is provided in general [Liew et al., 2019; Chua et al., 2020]. For instance, for the tested specimens in Dai et al. [2019], the moment resistances of the inter-module connections were

around 8% of the yield moment resistance of the column section, and the rotational stiffnesses of the inter-module connections were less than $0.5EI_c/L_c$, which is very close to nominally pinned. The outcome is that columns are not continuous in terms of bending moment transfer between upper and lower modules. In terms of the requirement on rotational stiffness of inter-module connections in seismic design, limited research has been conducted and no design guideline has been available.

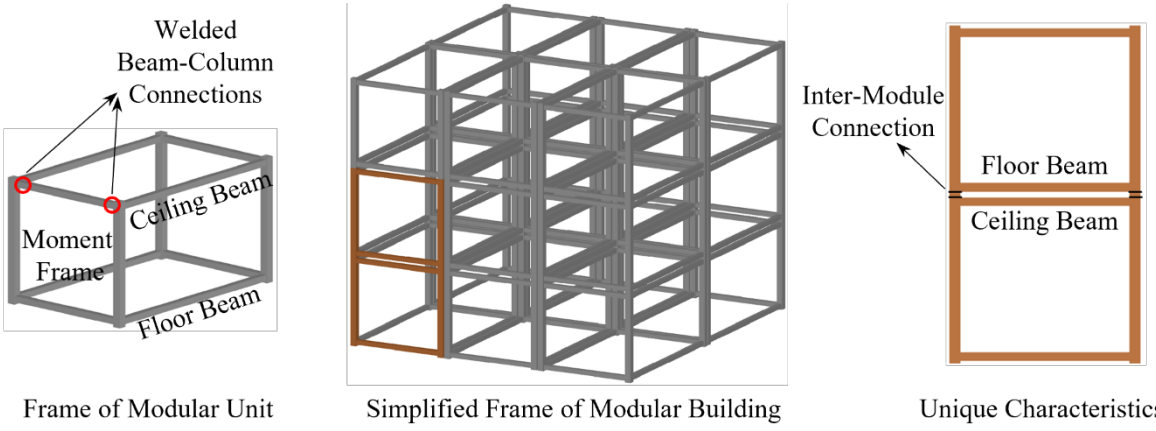

Fig. 1. Modular building with steel frames

Previous studies have revealed that, due to the unique structural characteristics mentioned above, different seismic behavior is expected from modular buildings as compared with conventional buildings. Conventional seismic design methods may not be applicable to modular buildings, as in some respects conventional methods do not account for the unique characteristics of modular buildings. Annan et al. [2009a] experimentally studied the behavior of a steel modular frame with diagonal braces, in which the design and construction of the test specimen accounted for the unique detailing requirements of modular buildings. Severe bending deformation was observed in the column segment between the ceiling beam and floor beam, while braced did not undergo much deformation. In Annan et al. [2009b] and Fathieh & Mercan [2016], several modular buildings with steel braced frames were designed following the conventional seismic design method, and nonlinear response history analyses under a set of ground motion records were conducted. Severe concentration of inelasticity in one story was reported in both studies. They

concluded that one key reason was that the insufficient rotational connectivity between columns limited the redistribution of internal forces from one module to another. Srisangeerthanan et al. [2018] studied the effect of diaphragm discontinuity on the seismic response of modular steel buildings. They found that the increased diaphragm flexibility led to dramatically larger inter-story drift and the inertial forces were considerably different from calculated values using the equivalent lateral force procedure in current seismic codes.

Currently there are no seismic design methods available that are tailored for modular buildings to account for their unique characteristics. In this paper, a new seismic design method, namely, the distributed seismic design method, is proposed specifically for modular buildings with steel frames. The distributed seismic design method is intended to account for the unique characteristics of modular buildings and to make use of the inherent significant lateral resistance in the steel frame of all modules. A 9-story prototype building was designed following the proposed method, and a numerical parametric study was conducted. Based on the validated numerical modeling method, 24 models were created to study the effect of three parameters, i.e., the rotational stiffness of inter-module connections, the seismic design force level, and the height-wise distribution of the design base shear. Firstly, the fundamental natural periods of the steel modular frames were studied through the linear elastic analysis. Subsequently, through the nonlinear static (pushover) analysis, the plastic mechanisms of the structure under lateral loading were evaluated. Last, nonlinear response history analyses (NRHAs) under 22 ground motion (GM) records were conducted for each model. The effect of different parameters on the collapse prevention performance was investigated.

2 Distributed seismic design method

2.1 Concept of the distributed seismic design

With building modules prefabricated in controlled environment and the increasing adoption of automatic welding robots, beams are typically welded to columns with high quality for modules

with steel frames. Under the new normal, the frame of each module is effectively a moment-resisting frame that can provide significant lateral resistance [Liu et al., 2020], as illustrated in Fig. 2(b). By exploiting the lateral resistance of all the modules, the concept of distributed seismic design is proposed in this study. Under the new concept, the frames of all modules are part of the seismic force resisting system (SFRS) and will contribute to the lateral resistance for the whole building, as illustrated in Fig. 2(a).

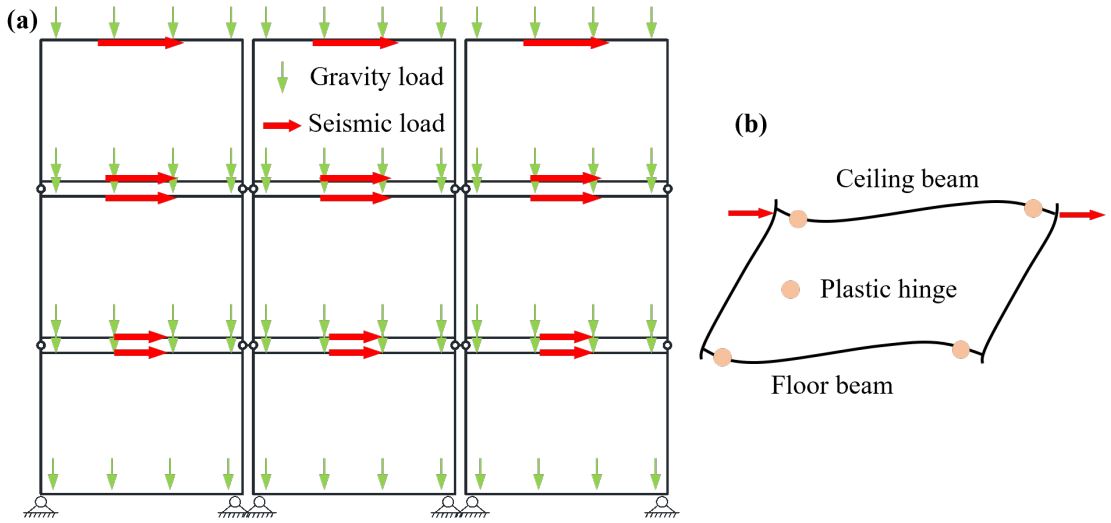

Fig. 2. (a) Seismic load resisted by all modules; (b) Deformation of the moment frame of one module to resist lateral load

In the seismic design of conventional buildings, only a few SFRSs (either braced frames, moment frames, or shear wall systems, etc.) are generally adopted in each principal direction of the building. The seismic inertial forces have to be transferred in the floor diaphragm to the SFRSs before being transferred to the ground. Compared with the conventional seismic design, the distributed seismic design can provide the following advantages:

(1) The seismic inertial forces originated from the dynamic effect on the mass can be transferred to the ground directly by the module frame to which it belongs. In other words, the seismic force does not have to be transferred horizontally in the floor plane first to the SFRS before being transferred to the ground. This advantage is of particularly benefit for module buildings because floor diaphragms are usually discontinuous and horizontal force transfer within the building relies mainly on inter-module connections.

115 (2) With the design seismic force distributed to all modules, uniform structural design will
116 be needed for repetitive modules at the same story. Even for structural design of modules at
117 different stories, less variation would be expected because gravity loads (almost the same for all
118 modules) play a more significant role in the distributed seismic design than in conventional seismic
119 design. Uniform and standardized structural design is particularly preferred by the fabrication of
120 modules in factory as it means no modification in the fabrication procedure, fewer types of
121 materials and steel sections, less material waste, and therefore less error and shorter fabrication
122 period.

123 (3) More seismic redundancy will be achieved with the lateral resistance distributed in all
124 modules. In other words, the failure of one or a few components will not result in much loss in the
125 lateral resistance of the whole modular building structure.

126 **2.2 Design method**

127 Following the distributed seismic design concept, a design method based on the conventional
128 seismic design framework with modifications was proposed, as elaborated below. Firstly, the
129 seismic design force (also termed 'seismic design base shear' in some codes) was determined and
130 distributed over the height of the building. For determination of the seismic design force, similar
131 parameters have been adopted in different codes to account for the nonlinear behavior of structures
132 under earthquake loading, for instance, the seismic response modification factor, R, in ASCE/SEI
133 7 [ASCE, 2016] and the structural behavior factor, q, in Eurocode 8 [CEN, 2004]. Due to the lack
134 of research, the optimum seismic design force level (i.e., the optimum value of R or q) has not
135 been quantified. In the case study presented in the following sections, two trial values of R will be
136 adopted to study the effect of different seismic design force levels. Moreover, two height-wise
137 distribution of the design base shear will be considered in the following parametric study.

138 Subsequently, the capacity-based design method was adopted to conduct the structural
139 design. With the similarity of the steel modular frame to the traditional moment-resisting frame, it

140 is proposed that the modular frame develops inelastic lateral deformation through the formation of
141 plastic hinges at beam ends and the columns are designed to be stronger than the fully yielded and
142 strain-hardened beams.

143 The beam sections were first determined through linear static analysis of the structure under
144 the combined gravity load and the design seismic load. As explained in Introduction, most existing
145 inter-module connections have limited bending moment transfer capacity. For the structural design
146 in this study, inter-module connections are assumed to be pinned. By assuming the moments at
147 beam ends reach the expected flexural strength of the respective beam ($M_{\mathrm{exp,b}}$), the force demands
148 on the columns can be determined accordingly, as shown in Fig. 3. The expected flexural strength
149 of the beam as determined as

$$M_{\mathrm{exp,b}} = R_{\mathrm{y}} M_{\mathrm{p,b}} \tag{1}$$

150 where $M_{\mathrm{p,b}}$ is the plastic moment resistance of the beam based on the specified minimum yield
151 strength and R_{y} is the ratio of the expected yield strength of the steel to the specified minimum
152 yield strength in line with AISC 341 [AISC, 2016]. As corner columns are common to the two
153 frames in the orthogonal planes, their design shall be designed based on the demands from the two
154 frames assuming earthquake strikes in either of the two principal directions.

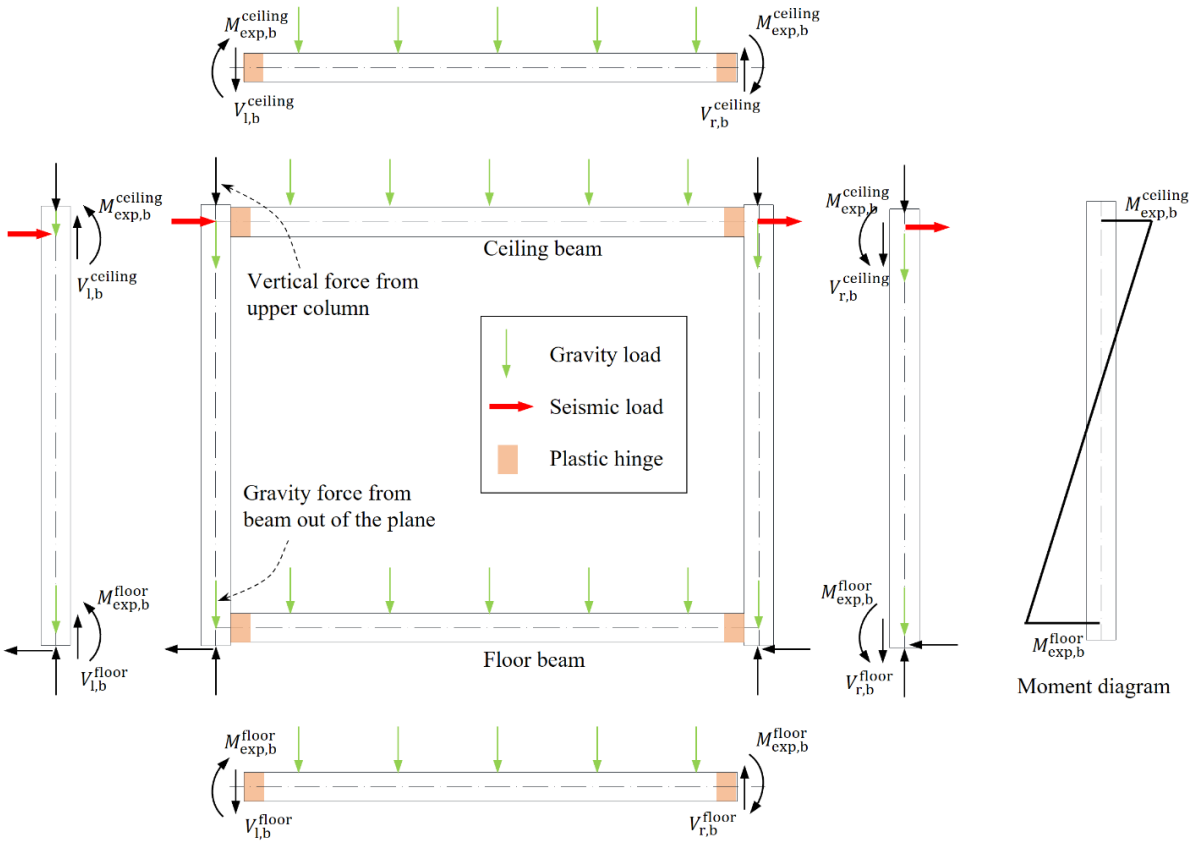

Fig. 3. Capacity-based design of the modular frame with plastic hinges at beam ends

3 Case study

3.1 Prototype building

A 9-story prototype modular residential building with steel frames was studied. The plan view of the building and the dimensions of each module are shown in Fig. 4. A distance of 200 mm is assumed between centerlines of the adjacent ceiling beam and floor beam. The design gravity loads are listed in Table 1, where the dead load consists of the self-weight of structural elements and the superimposed dead load of utilities and finishes. A line load of 5 kN/m on floor beams is also considered to account for the light-weight infill walls. The seismic weight was determined as $1.0D+0.5L$.

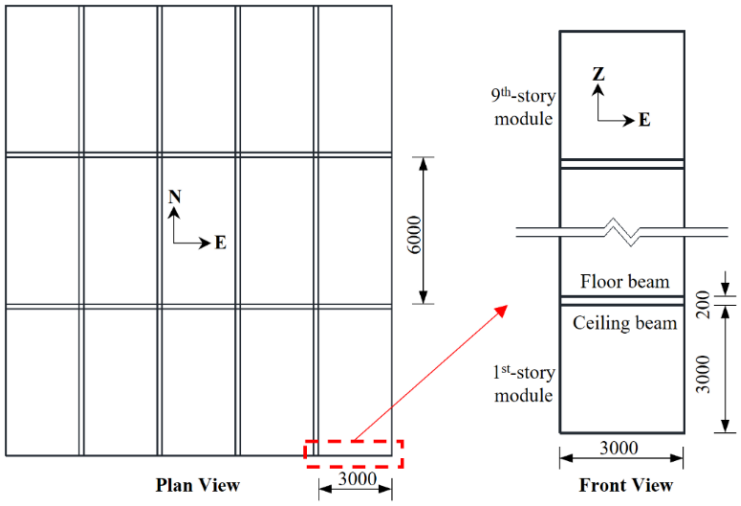

Fig. 4. Dimensions of the 9-story prototype building with repetitive module layout and the frame of one stack of modules

Table 1. Gravity loads and seismic parameters

		Dead load (D)	Live load (L)
Gravity load	Roof	4 kN/m^2	1 kN/m^2
	Floor slab	4 kN/m^2	2 kN/m^2
	Ceiling slab	2.5 kN/m^2	0
	Floor beam	5 kN/m	-
Seismic parameters	Seismic Design Category (SDC): C Site class: C S_{DS} = 0.5g S_{D1} = 0.2g Importance factor = 1.0		

The seismic hazard was quantified according to ASCE/SEI 7 [ASCE, 2016]. The building was intended to be located in a moderate seismic region with site class C. In particular, the Seismic Design Category is C with the short-period response acceleration parameter (S_{DS}) of 0.50g and 1-second response acceleration parameter (S_{D1}) of 0.20g. The load combinations considered in the structural design include: 1.4D, 1.2D+1.6L, 1.2D+ E_v+ E_h +L, and 0.9D- E_v+ E_h, where E_h and E_v are horizontal and vertical seismic load, respectively. The vertical seismic load was determined in accordance with ASCE/SEI 7 [ASCE, 2016].

The structure design was conducted following the procedure described in Section 2. The seismic behavior in the East-West direction of the building was studied. As the prototype building has repetitive module layout in each story, the mass and the seismic force are assumed to be

distributed equally to each module. Following the distributed seismic design method, the structural design of all modules in the same story was the same. Consequently, each stack of modules is expected to experience the same response under earthquake excitations in the East-West direction, which will be discussed further in Section 4.2. As such, the frame of only one stack of modules was considered in the following numerical analyses, whose front view is shown in Fig. 4.

3.2 Parametric study

For the seismic design of steel moment frames, a response modification factor (R) in the range of 3 to 8 is specified in ASCE/SEI 7 [ASCE, 2016], depending on the seismic design method. With the similarity of steel modular frames to the conventional steel moment frames, two trial values within the range, specifically, 3 and 6, were considered for the response modification factor (R) to study the effect of different seismic design force levels. For the calculation of design base shear, the fundamental period (T_a) calculated by the empirical formula in ASCE/SEI 7 [ASCE, 2016] was used.

The current height-wise distribution of design base shear in building codes are generally based on 1st-mode dynamic solution of the corresponding lumped-mass system assuming a linear mode shape [Chao et al., 2007], which can be expressed as

$$F_i = V\frac{w_x h_x}{\sum_{i=1}^{n} w_i h_i} \tag{2}$$

where F_i is the lateral force at the i^{th} level, V is the design base shear, w_i is the lumped seismic mass at the i^{th} level, h_i is the height of the i^{th} floor. To account for the higher-mode effect, other distributions have been proposed, for instance, the addition of a concentrated lateral force (F_t) at the top level [NRCC, 2015], which is expressed as

$$F_i = (V - F_t)\frac{w_x h_x}{\sum_{i=1}^{n} w_i h_i} \tag{3}$$

To study the effect of different height-wise distribution of the design base shear, both the distributions expressed in Eqs 2 and 3 were considered in the design of the prototype building, referred to as 1st-Mode distribution and Higher-Mode distribution, respectively. For consistent

comparison, the concentrated lateral force (F_t) at the top level was taken as $0.25V$ in all cases where the Higher-Mode distribution was adopted.

After determination of the required strength demands, the sections of beams and columns were selected in accordance with the provisions in AISC 360 [AISC, 2016]. Rectangular or square steel hollow structural sections (HSSs) categorized as Highly Ductile were adopted in order for ductile behavior of plastic hinges under severe earthquakes. The steel grade for the HSSs is ASTM A500 Grade C with the minimum specified yield strength of 345 MPa. The structural design results of the prototype building are listed in Appendix A.

Under strong earthquakes, the rotational connectivity of inter-module connections may help to redistribute the plastic lateral drifts over the building height [MacRae et al., 2004]. To study the effect of rotational stiffness of the inter-module connections, 6 different rotational stiffnesses were studied. The two extreme cases are pinned and rigid, with the corresponding stiffness of the rotational spring of zero and infinity, respectively. Four other stiffnesses in between as illustrated in Fig. 5 were included. They are differentiated by the rotation (θ) of the inter-module connection when the bending moment reaches the plastic moment resistance ($M_{\mathrm{p,c}}$, calculated based on the specified minimum yield strength and plastic section modulus) of the connected upper column section. For instance, the term 'K20' denotes the stiffness of the inter-module connection that will rotate by 20% radians under the bending moment of $M_{\mathrm{p,c}}$. For convenience of reference, all the cases in the parametric study are labeled and their meanings are listed in Table 2.

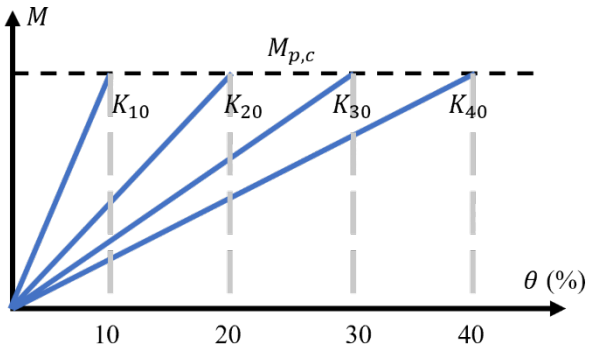

Fig. 5. Definition of terms for rotational stiffness of inter-module connections

Table 2. Study cases in the parametric study

Model ID	*R*	Height-wise distribution	Rotational stiffness
R3-1st-Pin	3	1st-Mode distribution	Pin
R3-1st-K40	3	1st-Mode distribution	K40
R3-1st-K30	3	1st-Mode distribution	K30
R3-1st-K20	3	1st-Mode distribution	K20
R3-1st-K10	3	1st-Mode distribution	K10
R3-1st-Rigid	3	1st-Mode distribution	Rigid
R3-Higher-Pin	3	Higher-Mode distribution	Pin
R3-Higher-K40	3	Higher-Mode distribution	K40
R3-Higher-K30	3	Higher-Mode distribution	K30
R3-Higher-K20	3	Higher-Mode distribution	K20
R3-Higher-K10	3	Higher-Mode distribution	K10
R3-Higher-Rigid	3	Higher-Mode distribution	Rigid
R6-1st-Pin	6	1st-Mode distribution	Pin
R6-1st-K40	6	1st-Mode distribution	K40
R6-1st-K30	6	1st-Mode distribution	K30
R6-1st-K20	6	1st-Mode distribution	K20
R6-1st-K10	6	1st-Mode distribution	K10
R6-1st-Rigid	6	1st-Mode distribution	Rigid
R6-Higher-Pin	6	Higher-Mode distribution	Pin
R6-Higher-K40	6	Higher-Mode distribution	K40
R6-Higher-K30	6	Higher-Mode distribution	K30
R6-Higher-K20	6	Higher-Mode distribution	K20
R6-Higher-K10	6	Higher-Mode distribution	K10
R6-Higher-Rigid	6	Higher-Mode distribution	Rigid

227
228

229 ## 4 Numerical modeling

230 ### 4.1 Validation of numerical modeling method

231 To develop and validate the numerical modeling method that is to be adopted in the following
232 parametric study, numerical models were developed for the experimental test specimens reported
233 in Dai et al. [2019]. As shown in Fig. 6, the test specimens consisted of all the essential components
234 that form the modular frames, i.e., floor and ceiling beams, columns, and inter-module connections,
235 which are therefore deemed appropriate for validation of numerical models in this study.

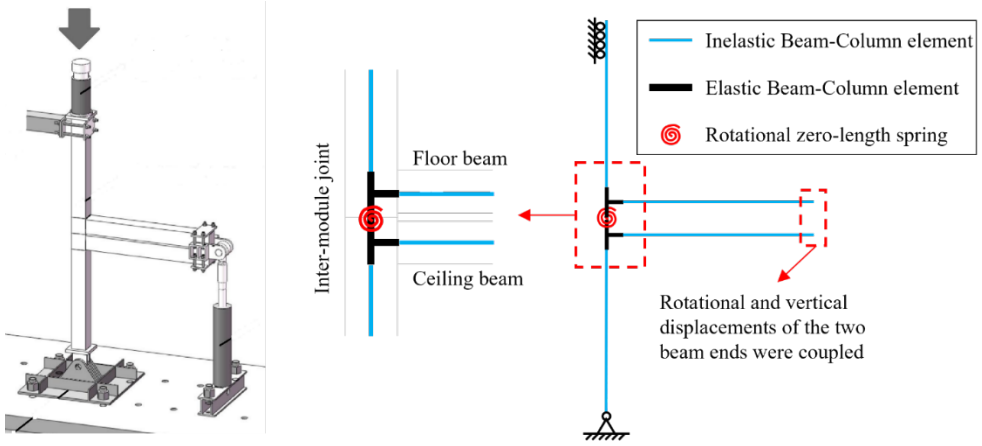

(a) (b)

Fig. 6. (a) Test setup for the modular structure subassembly [Dai et al., 2019]; (b) Numerical model

Two-dimensional numerical models were developed in OpenSees [McKenna, 1997]. Beams and columns were modeled using displacement-based beam-column elements with fiber-based sections replicating the corresponding geometric dimensions [Wang et al., 2021; Xu et al., 2022]. For discretization of structural elements and fiber-based sections, at least 8 elements for each beam and column, 10 fibers along the section width/height and 4 fibers through the section thickness were used. Rigid connection was assumed for the welded beam-to-column connections. Due to the strengthening of the beam-to-column joints typical of modular structures, e.g., the addition of joint box and end plates in Dai et al. [2019], the beam-to-column joints usually remain elastic. As such, the beam-to-column joints were modeled elastic in this study. For each inter-module connection, an elastic rotational spring was adopted to capture the behavior under bending. The stiffness of the rotational spring was determined following the guidance in Dai et al. [2019].

The steel material was modeled using the Steel02 uniaxial material model. The tension coupon test results were used to define the yield strength (F_y = 393.8 MPa) and the strain hardening ratio (b = 0.35%). Recommended values for typical steel material were adopted for other parameters [Mazzoni et al., 2009], specifically, R0 = 15, cR1 = 0.925, cR2 = 0.15. The boundary conditions were set consistent with those in the test; loading was applied following the loading protocol prescribed in the literature [Dai et al., 2019].

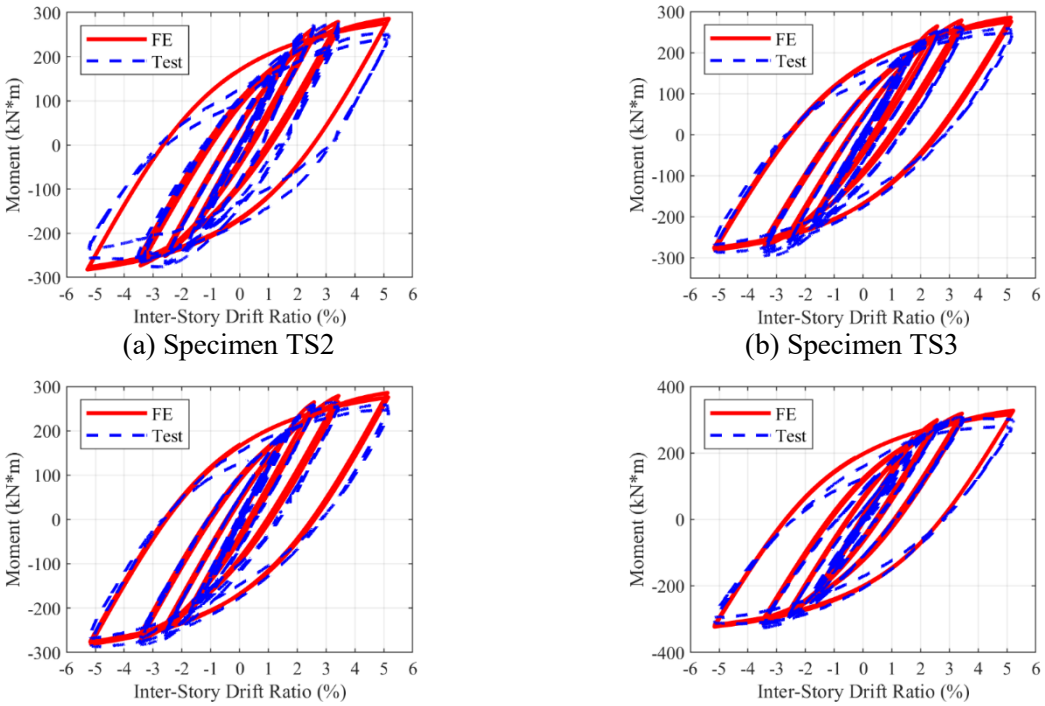

(a) Specimen TS2 (b) Specimen TS3

(c) Specimen TS4 (d) Specimen TS5

Fig. 7. Comparison between the numerical and experimental results

As shown in Fig. 7, a good match was obtained between the numerical and experimental results up to the inter-story drift ratio (IDR) of 5%. It implies that the adopted numerical modeling method could capture the behavior of steel modular frames up to IDR of 5% with satisfactory accuracy.

4.2 Numerical modeling of the prototype building

The numerical modeling of the structure followed the validated method described in Section 4.1. The yield strength was set as the expected yield strength for ASTM A500 Grade C as specified in AISC 341 [AISC, 2016], i.e., 1.3×345 = 448 MPa, where 1.3 is the ratio of the expected yield strength to the specified minimum yield strength. Other parameters were the same as those adopted in the validation models. The Rayleigh damping was adopted with the modal damping ratio set as 2% for the first two modes.

To study the possible interaction between different stacks of modules of the prototype building through horizontal inter-module connections, a numerical model was first constructed for a structure with 3 modules in each of X, Y, Z directions as shown in Fig. 8(a). For the horizontal

inter-module connections, the configuration reported in Chua et al. (2020) was assumed, and the modeling method recommended in Chua et al. (2020) was followed in the numerical models. For comparison, a numerical model for one stack of modules was also constructed as shown in Fig. 8(b). Both the structure of 3×3 stacks of modules and the structure of one stack of modules were taken from the bottom three stories of the prototype building.

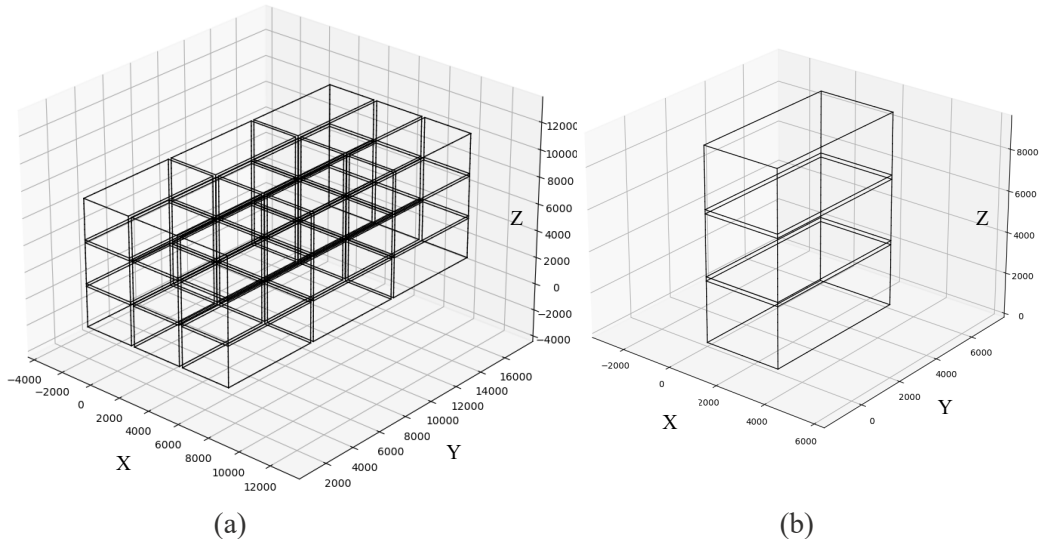

(a) (b)

Fig. 8. (a) Structure of 3×3 stacks of modules; (b) Structure of one stack of modules

The vibration modes of the two structures were studied through modal analyses. The first three modal shapes and corresponding periods are presented in Fig. 9. As shown, the first and second modal shapes and the associated periods of the structure with 3×3 stacks of modules are the same as those of the structure with one stack of modules. This is because the structure of 3×3 stacks of modules is the 3×3 repetition of one stack of modules and no strong interaction between modules is expected under the lateral vibration. However, the two structures have different torsional vibration modes and associated periods. This is because under torsional vibration, the whole building tends to rotate around the center of the building and different stacks of modules will deform differently. In this case, strong interaction will be involved between modules through horizontal inter-module connections. In contrast, the rotation of one stack of modules will be around the center of the module without influence of adjacent stacks of modules.

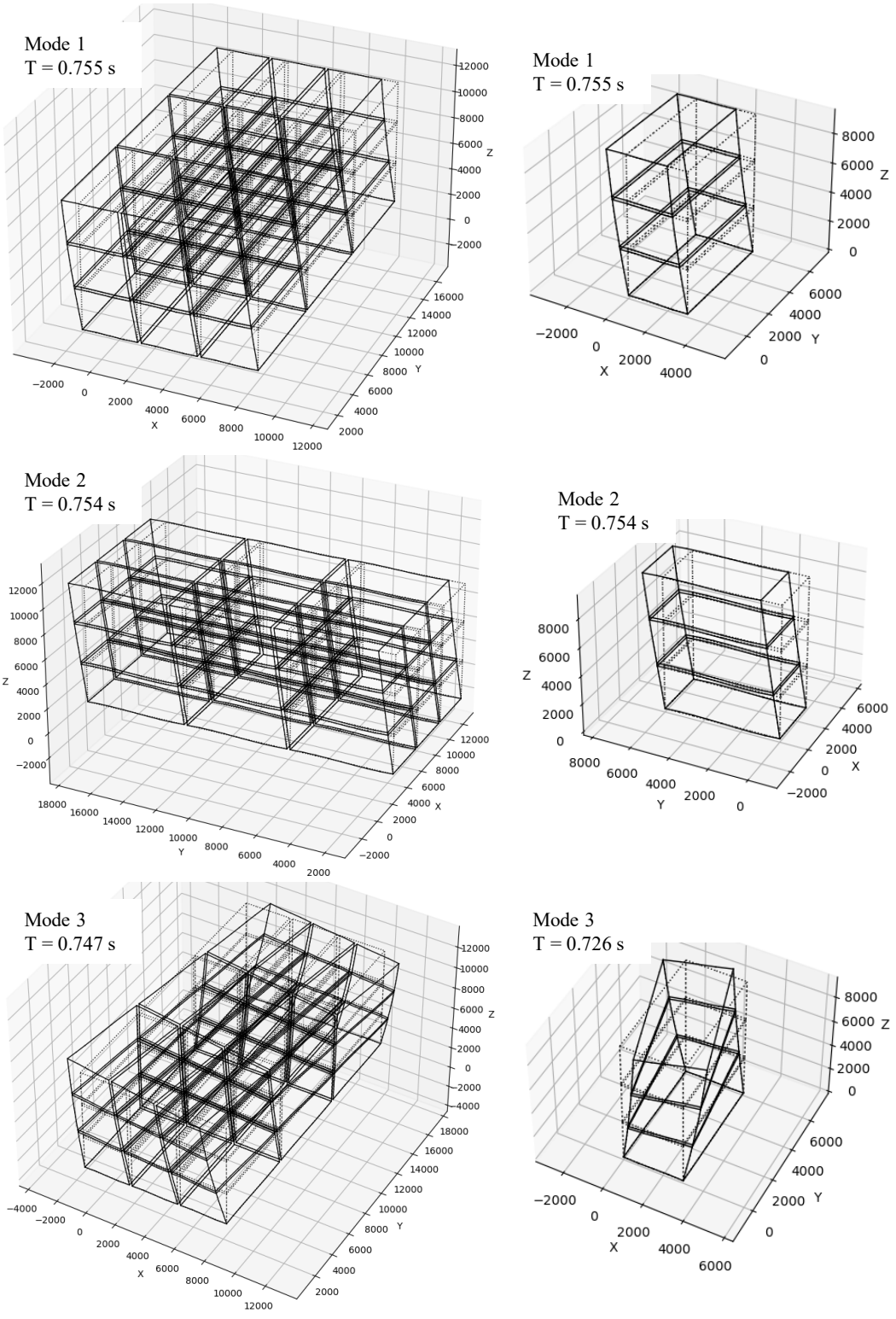

Fig. 9. First three modal shapes and periods

As the prototype building has a regular plan and the dimensions of all modules are the same, not much torsional response will be expected. The lateral vibration modes and periods of one stack of modules will be representative of those of the whole prototype building. Under earthquake

294 excitations in one principal direction of the building, the same response will be expected for
295 different stacks of modules. As such, the frame of only one stack of modules was studied for the
296 prototype building, whose numerical model is shown in Fig. 10.

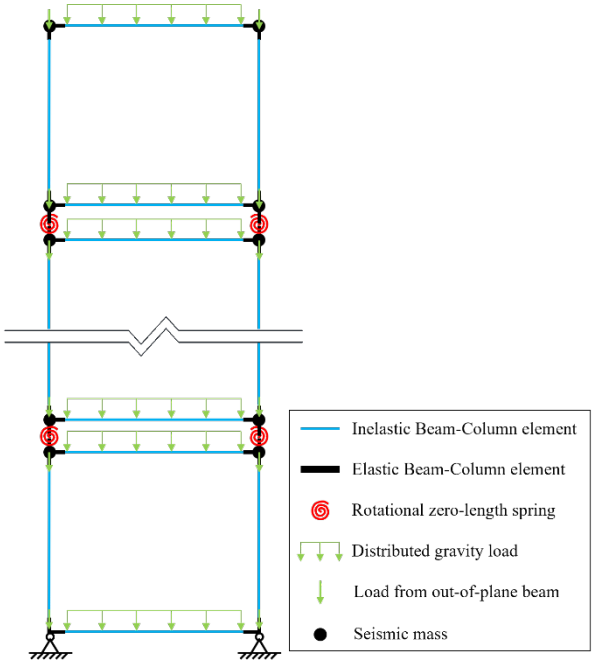

297

298 **Fig. 10.** Numerical model of the modular structure

299 **4.3 Natural periods of modular frames**

300 The periods for the first three modes of vibration of modular frames were determined through
301 eigenvector analyses and listed in Table 3. The modal participating mass ratio (MPMR) associated
302 with each mode was also listed in Table 3. Fig. 11 (a) and (b) show the first three modal shapes
303 for the model R3-Higher with pinned inter-module connections and with rigid inter-module
304 connections, respectively. It was found that the rotational stiffness has little impact on both the
305 first (also called fundamental) and second periods. This is because under the first and second
306 vibration modes, the rotation of the inter-module connections is limited, and the rotational stiffness
307 of inter-module connections therefore does not contribute much to the lateral stiffness of the whole
308 frame. Under the third (and higher) vibration mode, more rotation of inter-module connections is
309 involved, and increasing rotational stiffness will result in higher lateral stiffness and shorter
310 associated period.

311 As expected, natural periods of the structure designed with R=3 (i.e., higher seismic design
312 force level) are shorter than in the case of R=6. This is because strength and stiffness are usually
313 correlated, and a stiffer structure is often resulted when designed for a higher seismic force level.
314 Likewise, periods of structures designed following the Higher-Mode distribution of the design
315 base shear are slightly shorter than when the 1st-Mode distribution was considered. This is because
316 the design shear force demands, especially in upper stories, are generally larger under the Higher-
317 Mode distribution. It is worth noting that only the contribution of structural elements to the
318 stiffness was considered in the calculation of fundamental periods. Further experimental study is
319 needed to evaluate the actual fundamental periods of modular buildings with steel frames with the
320 consideration of stiffness contribution from non-structural elements, e.g., infill walls.

321 **Table 3.** Natural periods and modal participating mass ratios (MPMRs) of the modular frames

Model			Pin	K40	K30	K20	K10	Rigid
R3-1st	Mode 1	Period (s)	2.92	2.92	2.92	2.92	2.92	2.91
		MPMR	0.76	0.76	0.76	0.76	0.76	0.76
	Mode 2	Period (s)	1.19	1.19	1.19	1.19	1.19	1.14
		MPMR	0.13	0.13	0.13	0.13	0.14	0.14
	Mode 3	Period (s)	0.75	0.75	0.75	0.74	0.74	0.64
		MPMR	0.04	0.04	0.04	0.04	0.04	0.05
R3-Higher	Mode 1	Period (s)	2.80	2.80	2.80	2.80	2.80	2.79
		MPMR	0.79	0.79	0.79	0.79	0.79	0.79
	Mode 2	Period (s)	1.06	1.06	1.06	1.05	1.05	1.01
		MPMR	0.13	0.13	0.13	0.13	0.13	0.12
	Mode 3	Period (s)	0.65	0.64	0.64	0.63	0.62	0.57
		MPMR	0.04	0.04	0.04	0.04	0.04	0.04
R6-1st	Mode 1	Period (s)	4.27	4.26	4.26	4.26	4.25	4.21
		MPMR	0.79	0.79	0.79	0.79	0.79	0.78
	Mode 2	Period (s)	1.63	1.62	1.62	1.61	1.60	1.56
		MPMR	0.12	0.12	0.12	0.12	0.12	0.12
	Mode 3	Period (s)	1.02	1.00	0.99	0.98	0.95	0.85
		MPMR	0.04	0.04	0.04	0.04	0.04	0.04
R6-Higher	Mode 1	Period (s)	4.06	4.05	4.05	4.04	4.03	3.99
		MPMR	0.81	0.81	0.81	0.81	0.81	0.80
	Mode 2	Period (s)	1.51	1.49	1.49	1.48	1.47	1.40
		MPMR	0.11	0.11	0.11	0.11	0.11	0.11
	Mode 3	Period (s)	0.90	0.88	0.87	0.86	0.85	0.77
		MPMR	0.04	0.04	0.04	0.04	0.04	0.04

322

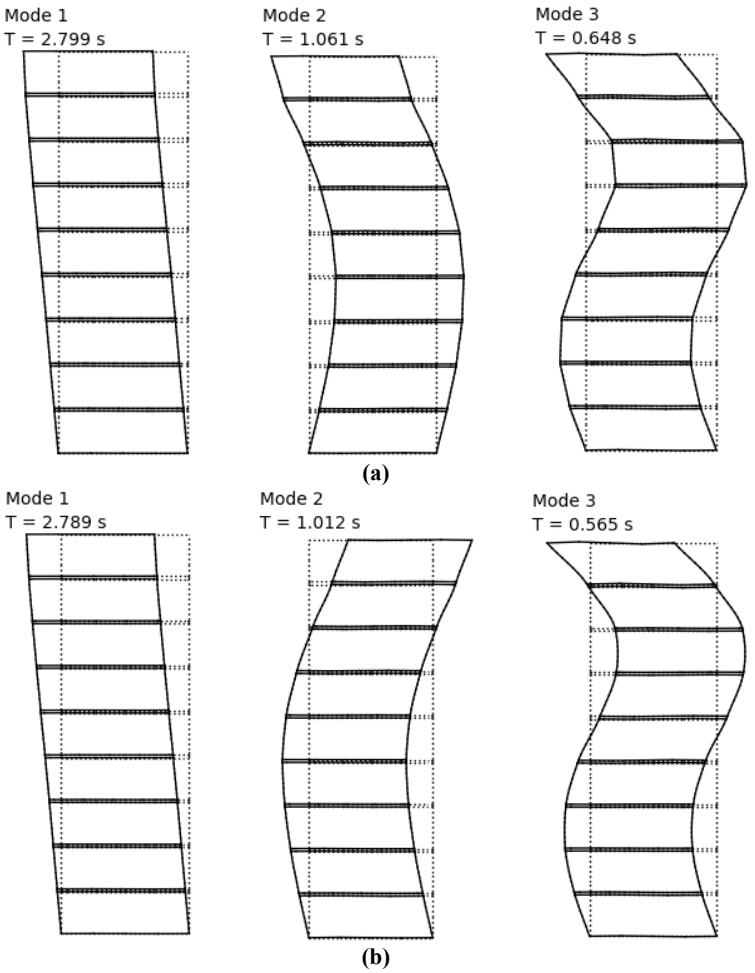

Fig. 11. Modal shapes of the modular frame: (a) Model R3-Higher with pinned inter-module connections; (b) Model R3-Higher with rigid inter-module connections

5 Inelastic static (pushover) analysis

The pushover analysis has been proven an effective and efficient method to provide insight into structural behavior under earthquake lateral loading [Krawinkler & Seneviratna, 1998]. Although the pushover results may not mimic accurately the dynamic response, they can be used to cross validate the nonlinear dynamic analysis results that will be presented in Sections 6.

For each model of the parametric study listed in Table 2, the frame was subject to lateral forces with an invariant height-wise distribution $m\Phi_1$, where m is the mass matrix of the idealized lumped-mass model, and Φ_1 is the 1st-mode shape obtained through the eigenvector analysis in Section 4.3.

Displacement control was applied to study the formation of the mechanism and the structural behavior after mechanism formation. As the roof displacements might not be monotonic in some cases (e.g., the 'roof backward phenomenon' discussed later on), the control node in the analysis was chosen at ceiling level of the 1st-story module. Fig. 12 shows the normalized global pushover (base shear-roof drift) curves for all the cases in the parametric study, in which the base shear is normalized to the weight of the structure, and the roof drift is normalized to the structural height.

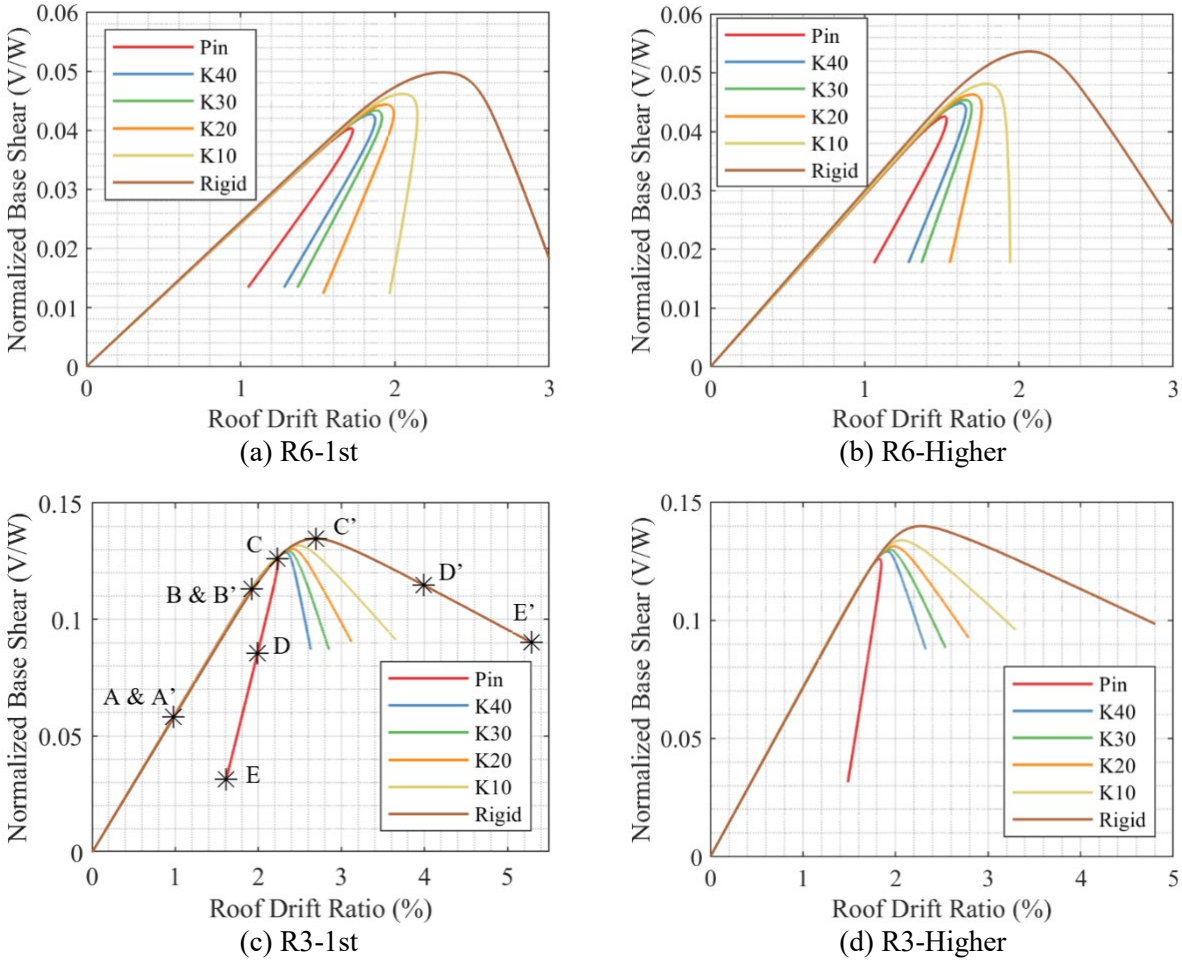

(a) R6-1st (b) R6-Higher

(c) R3-1st (d) R3-Higher

Fig. 12. Normalized global pushover curves for different models

For cases in each subplot, of which the only difference was the rotational stiffness of the inter-module connections, curves coincide in the initial linear branch, implying that these corresponding structures have the same global lateral stiffness. This further verifies the conclusion that the rotational stiffness of inter-module connections has limited impact on the elastic lateral stiffness and therefore the fundamental period of the steel modular frames.

For all the models, after yielding occurs, the base shear reached a peak value, and then declined at different rate without plateau. Two behavioral patterns can be identified for the structures in the parametric study. In the first pattern, the roof drift continues increasing with the declined base shear, which resulted in the 'negative stiffness' branch in the global base shear-roof drift curve. The 'negative stiffness' behavior was mainly due to the P-delta effect and the reduced lateral stiffness caused by plastic deformation in some modules. Fig. 13(a) shows the deformation of the model R3-1st-Rigid at the point E' of the corresponding pushover curve. The inter-story drift development of the 9 stories throughout the pushover analysis were also plotted in Fig. 14(a) for R3-1st-Rigid, with key steps corresponding to the points on the global pushover curve noted. The inter-story drift ratio (IDR) for the modular frame is defined as the ratio of the drift difference between the ceiling and the floor to the module height in this study. As shown, after the peak base shear reached, significant plasticity developed, especially in the lower modules, which led to substantial loss in the lateral stiffness of these stories. Due to the P-delta effect, the lateral load had to be decreased with the increase in the drift to keep the stability of the structure.

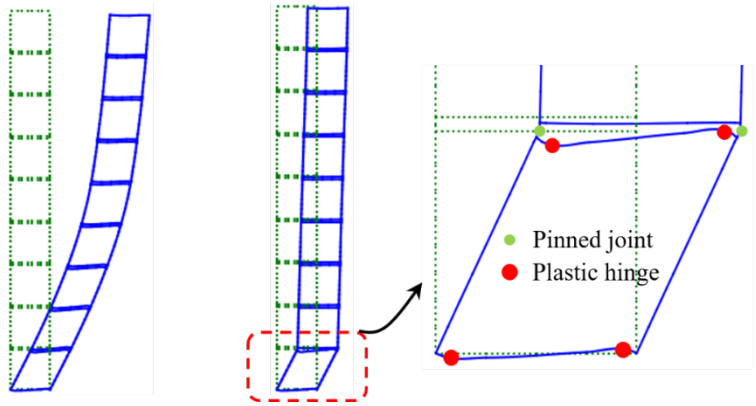

(a) (b)

Fig. 13. Deformation at the end of pushover analysis: (a) R3-1st-Rigid; (b) R3-1st-Pin and the soft-story mechanism (deformation amplification factor = 5)

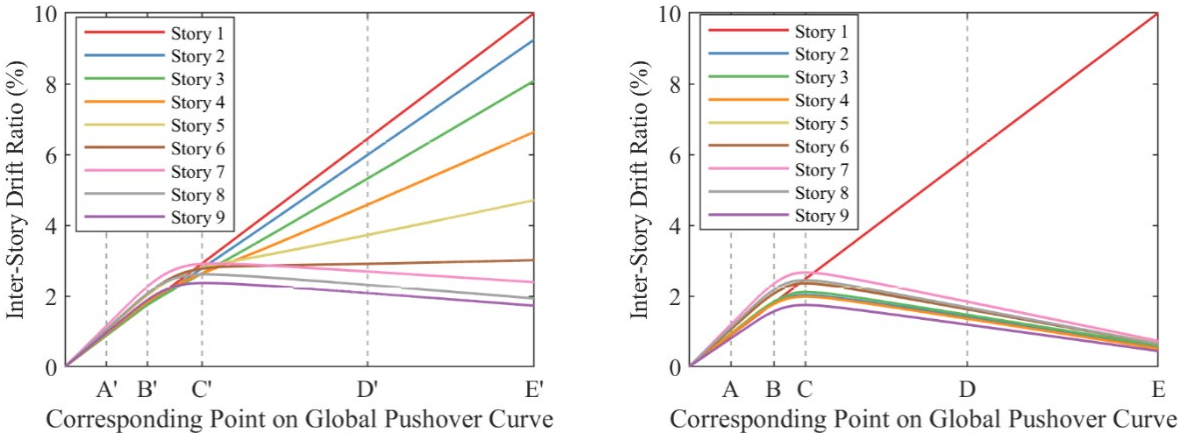

(a) R3-1st-Rigid (b) R3-1st-Pin

Fig. 14. Inter-story drift development of the 9 stories during the pushover analysis

In the second pattern, after the base shear reached the peak, the roof drift decreased, that is, the roof moved backward. This phenomenon is termed 'roof backward phenomenon' in this study. To illustrate the phenomenon, the inter-story drift development of the 9 stories throughout the pushover analysis were plotted in Fig. 14(b) for R3-1st-Pin. As shown, in the elastic phase, the story drifts are similar and increased with the almost same rate. However, after the base shear reached the peak, the story drift in the bottom module increased suddenly and a soft-story mechanism formed. Fig. 13(b) shows the deformation of R3-1st-Pin at the point E of the corresponding pushover curve. Due to the concentration of lateral deformation in the soft story and the P-delta effect, the lateral load declined sharply, which resulted in the story drift decline in other modules. The roof drift, which is the summation of drifts in all modules, as a result, decreased. The faster the roof moves backward, the more severe the drift concentration in the soft story is. The 'roof backward' behavior represents a higher level of drift concentration than the 'negative stiffness' behavior.

5.1 Effect of rotational stiffness of inter-module connections

The rotational stiffness of inter-module connections has a significant impact on the structural behavior when plasticity occurs. Firstly, with the increase in the rotational stiffness, the ultimate base shear was increased, indicating a higher level of overstrength. Secondly, strengthening the rotational stiffness could shift the post peak base shear behavior from 'roof backward' to 'negative

383 stiffness', indicating a less extent of drift concentration in the soft story. A comparison of Fig. 13(a)
384 and 13(b) shows visually that the drift concentration was significantly mitigated by changing the
385 inter-module connections from being pinned to rigid.

386 This is because, for modular frames with pinned inter-module connections, if the P-delta
387 effect is temporarily excluded, the lateral resistance of one module is independent of other modules
388 and can be estimated as

$$V_r = \frac{\sum M_{p,b}}{h_m} \tag{4}$$

389 where the numerator is the summation of the plastic moment resistances of four plastic hinges in
390 the beams (two in the floor beam and two in the ceiling beam), the denominator is the height of
391 the module. If the rotational stiffness of inter-module connections is increased, the lateral
392 resistance of one module will be increased, and the lateral deformation will be more distributed
393 because the deformation of adjacent modules will be mobilized. As the P-delta effect is
394 proportional to the lateral deformation, more severe drift concentration will therefore be obtained
395 for pinned inter-module connections. For all cases with pinned inter-module connections, the 'roof
396 backward' behavior was obtained, indicating the vulnerability of steel modular frames to drift
397 concentration in the soft story if pinned inter-module connections were used.

398 **5.2 Effect of seismic design force levels**

399 Comparison between the subplots of Fig. 12 shows that the smaller value of *R* (i.e., higher
400 seismic design force) could shift the post peak base shear behavior from 'roof backward' to
401 'negative stiffness' (e.g., R6-1st-K20 vs R3-1st-K20), or reduce the slope of the negative stiffness
402 branch (e.g., R6-1st-Rigid vs R3-1st-Rigid), implying a mitigation of the adverse P-delta effect.
403 This is because the relative importance of P-delta effect was decreased, which can be estimated by
404 the story stability coefficient

$$\theta = \frac{P\delta}{Vh} \tag{5}$$

where δ is the lateral drift under lateral load V, P is the gravity load, and h is the building height. With the gravity load and building height the same for all the structures, the larger lateral stiffness resulted from the higher seismic design forces lead to a lower value of the story stability coefficient.

6 Nonlinear response history analysis (NRHA)

NRHAs were conducted for all the structures designed in the parametric study to study the seismic behavior under maximum considered earthquakes (MCEs) with a returning period of 2475 years (corresponding exceedance probability of 2% in 50 years) [ASCE, 2016]. The focus was on collapse prevention performance and collapse evolution in case of collapse.

6.1 Ground motion (GM) selection and scaling

To account for the uncertainty in earthquake ground excitations, the set of 22 GM records developed in FEMA P695 [FEMA, 2009] was adopted in this study. The basic information about the GM set is listed in Table 4. The number of GM records is deemed sufficient to account for the variation in earthquake ground excitations. Moreover, the GM records were selected with the aim of being applicable to a variety of structural systems and different sites. More relevant information can be found in FEMA P695 [FEMA, 2009].

Following the scaling instructions, the GM records were scaled to match the seismic hazard of the prototype building specified in Section 3.1, by anchoring the median spectrum of the record set to the corresponding MCE spectral acceleration at 3.5 s. The MCE spectrum and the response spectra of individual scaled GM records are plotted in Fig. 15. The anchoring point was set at 3.5 s because it lies approximately halfway in the range of fundamental natural periods of the structures studied.

430 **Table 4.** Information of the ground motion record set [FEMA, 2009]

EQ ID No.	Earthquake			Recording Station	Source (Fault Type)
	M	Year	Name		
1	6.7	1994	Northridge	Beverly Hills - Mulhol	Thrust
2	6.7	1994	Northridge	Canyon Country-WLC	Thrust
3	7.1	1999	Duzce, Turkey	Bolu	Strike-slip
4	7.1	1999	Hector Mine	Hector	Strike-slip
5	6.5	1979	Imperial Valley	Delta	Strike-slip
6	6.5	1979	Imperial Valley	El Centro Array #11	Strike-slip
7	6.9	1995	Kobe, Japan	Nishi-Akashi	Strike-slip
8	6.9	1995	Kobe, Japan	Shin-Osaka	Strike-slip
9	7.5	1999	Kocaeli, Turkey	Duzce	Strike-slip
10	7.5	1999	Kocaeli, Turkey	Arcelik	Strike-slip
11	7.3	1992	Landers	Yermo Fire Station	Strike-slip
12	7.3	1992	Landers	Coolwater	Strike-slip
13	6.9	1989	Loma Prieta	Capitola	Strike-slip
14	6.9	1989	Loma Prieta	Gilroy Array #3	Strike-slip
15	7.4	1990	Manjil, Iran	Abbar	Strike-slip
16	6.5	1987	Superstition Hills	El Centro Imp. Co.	Strike-slip
17	6.5	1987	Superstition Hills	Poe Road (temp)	Strike-slip
18	7.0	1992	Cape Mendocino	Rio Dell Overpass	Thrust
19	7.6	1999	Chi-Chi, Taiwan	CHY101	Thrust
20	7.6	1999	Chi-Chi, Taiwan	TCU045	Thrust
21	6.6	1971	San Fernando	LA - Hollywood Stor	Thrust
22	6.5	1976	Friuli, Italy	Tolmezzo	Thrust

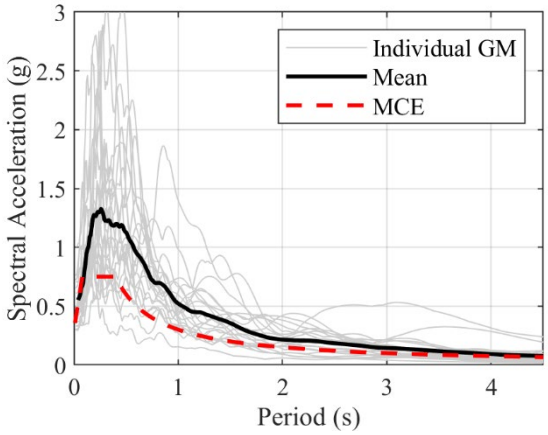

431

432 **Fig. 15.** Response spectrum of the selected and scaled GM set and MCE

6.2 Seismic response under certain GM record

The model R6-1st-Pin collapsed subject to GM 15, and its response is typical of the collapses exhibited by the structures studied. The inter-story drift ratio (IDR) histories of all the 9 stories are presented in Fig. 16(a). During the response cycle bounded by the black dashed lines, the IDR of the bottom module increased to a local peak of -5%, while the IDRs of other modules remained small. Severe plastic drift concentration in the bottom module occurred and a soft-story mechanism formed. The bottom module did not follow all the above modules to move back to its original position in the second half of the response cycle. During the following response cycle, the drift concentration in the bottom module increased further and structural instability finally occurred due to the large lateral drift and the P-delta effect. This collapse mechanism is consistent with the soft-story mechanism in the bottom module revealed through the pushover analysis.

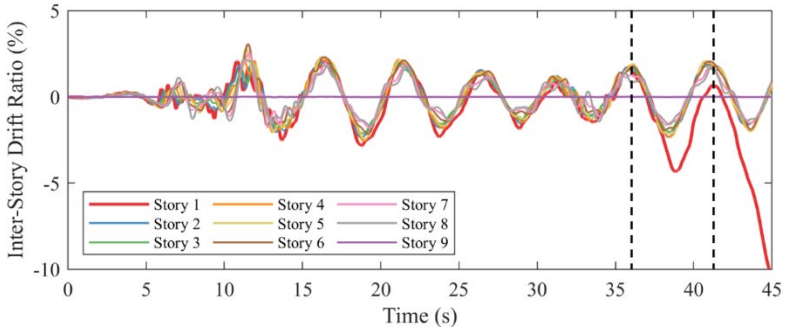

(a) R6-1st-Pin

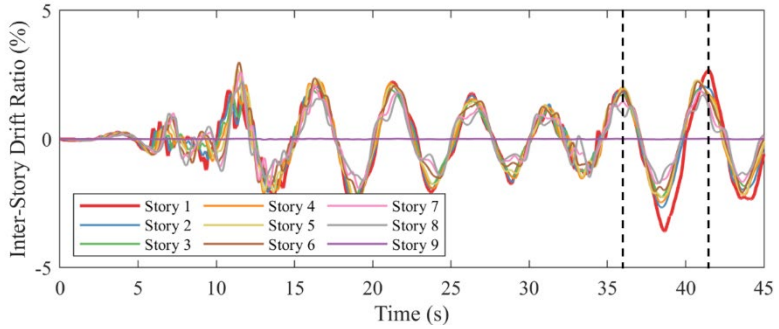

(b) R6-1st-K40

Fig. 16. Inter-story drift history of individual stories under GM 15

For purpose of comparison, the response of the model R6-1st-K40 under GM 15 is presented in Fig. 16(b). Collapse was prevented in this case. Almost the same behavior was obtained prior to the response cycle bounded by the black dashed lines. During the response cycle, the IDR of

448 the bottom module reached to a peak larger than those of all the other modules. However, the
449 difference between the peak IDRs was much smaller than in the model R6-1st-Pin, indicating a
450 less severe drift concentration. As the only difference of the model R6-1st-K40 from R6-1st-Pin
451 is the rotational stiffness of inter-module connections, it is believed that the rotational restraint by
452 the inter-module connections helped to mitigate the plastic drift concentration and avoid the
453 collapse eventually by mobilizing the lateral resistance of the upper modules.

454 **6.3 Effect of design parameters on collapse prevention**

455 The numbers of GM records under which collapse occurred are statistically studied to
456 examine the effect of the three parameters considered in the parametric study. Firstly, the collapse
457 criteria are pre-determined. In addition to the dynamic instability, the cases in which the IDR
458 exceeded 5% were also counted as collapse. The 5% drift limit is chosen for two reasons. First,
459 the nonlinear analyses were deemed to have sufficient accuracy to the IDR of approximately 5%.
460 Second, previous experiments indicate that most beam-to-column connections and columns do not
461 retain sufficient resistance beyond this drift level. Similar collapse criteria were used in other
462 studies [Fahnestock et al., 2007; Hsiao et al., 2013]. Based on the collapse criteria, the number of
463 GM records under which collapse occurred were examined for all the studied structures and
464 presented in Fig. 17.

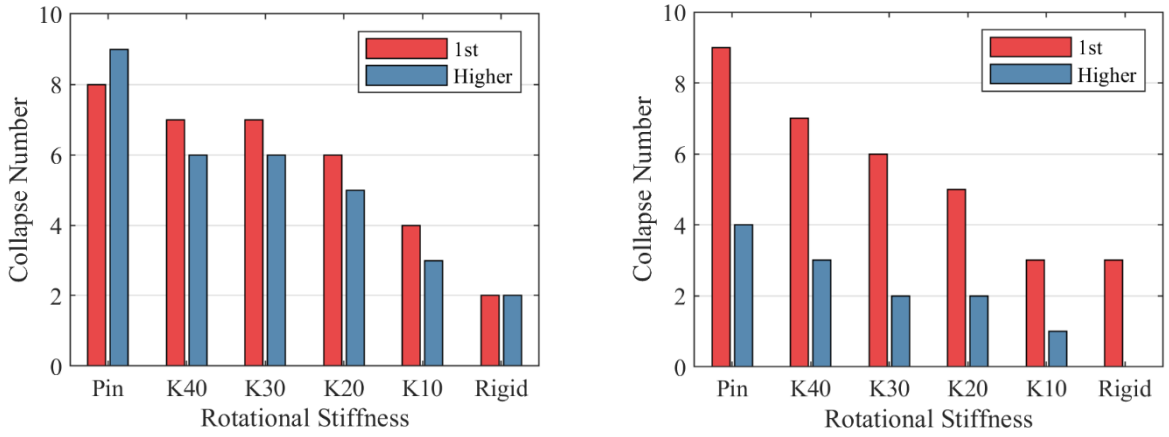

(a) R6 (b) R3

465 **Fig. 17.** Number of collapses out of 22 GM records

466 The most noticeable trend is that the number of collapses decreased with the increase in the
467 rotational stiffness of inter-module connections, irrespective of the seismic design force level and
468 the height-wise distribution of the design base shear. With the inter-module connections changed
469 from being pinned to rigid, the number of collapses decreased from 8 to 2, 9 to 2, 9 to 3, and 4 to
470 0, for the model R6-1st, R6-Higher, R3-1st, and R3-Higher, respectively. In light of the results of
471 the pushover analyses, it is believed that with the increase in the rotational stiffness of inter-module
472 connections, the lateral resistance of each module is no longer independent. The column bending
473 deformation in one module will be restrained by columns in the adjacent modules. As such, the
474 lateral drift concentration and the soft-story mechanism can be mitigated, if not eliminated, which
475 plays a crucial role in the collapse prevention of steel modular structures.
476 Comparison between Fig. 17(a) and 17(b) reveals that the effects of the seismic design force
477 level and the height-wise distribution of the design base shear cannot be evaluated in isolation. For
478 structures with R=6, the Higher-Mode distribution seemed not to have much impact on the number
479 of collapses. In contrast, for structures with R=3, the Higher-Mode distribution helped to reduce
480 the collapse number significantly. Likewise, for structures designed with the 1st-Mode distribution,
481 changing R from 6 to 3 resulted in little change in the number of collapses. However, for structures
482 designed with the Higher-Mode distribution, changing R from 6 to 3 resulted in substantial
483 reduction in the number of collapses.
484 The shape of the envelope of maximum IDRs may provide the insight into the tangled effect
485 of the seismic design force level and the height-wise distribution of the design base shear. Fig. 18
486 shows the envelopes of maximum IDRs under individual GMs for the four structures with rigid
487 inter-module connections. Also presented in Fig. 18 are the mean and mean plus one standard
488 deviation of maximum IDRs. As shown, for the two structures with R=6, a more uniform envelope
489 of maximum IDRs was obtained for the structure designed with the 1st-Mode distribution of the
490 design base shear. The respective structure designed with the Higher-Mode distribution exhibited

smaller maximum IDRs at upper stories but larger maximum IDRs at lower stories. This indicates that the seismic response of the R=6 structures was dominated by its 1st-mode response. The Higher-Mode distribution effectively strengthened the modules in the upper stories but made the lower modules relatively less stronger. In this case, the adoption of the Higher-Mode distribution did not lead to enhanced collapse prevention performance for the structure.

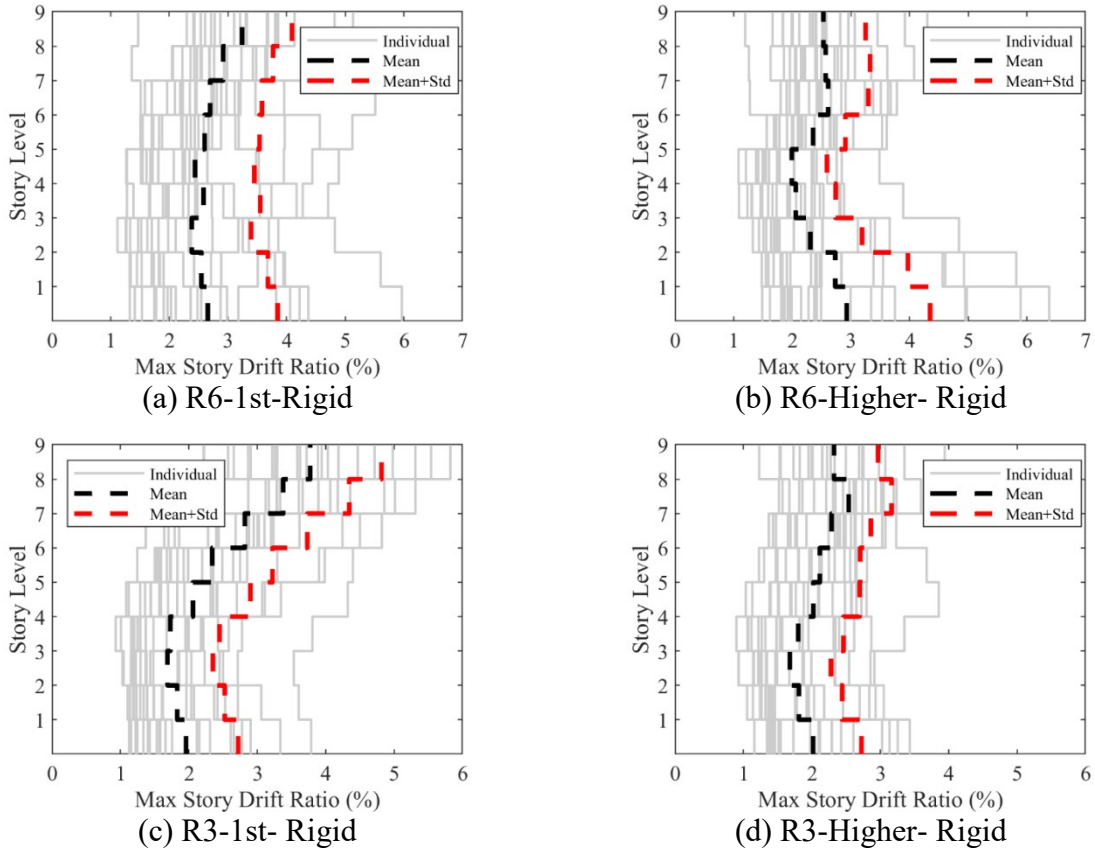

(a) R6-1st-Rigid (b) R6-Higher- Rigid

(c) R3-1st- Rigid (d) R3-Higher- Rigid

Fig. 18. Envelope of maximum IDRs

In contrast, for the two structures with R=3, a more uniform envelope of maximum IDRs was obtained for the structure designed with the Higher-Mode distribution of the design base shear, while the respective structure designed with the 1st-Mode distribution exhibited larger maximum IDRs at upper stories. This indicates that significant higher-mode responses were involved in the seismic response of the R=3 structures. The Higher-Mode distribution of the design base shear played a positive role in this case to account for the effect of higher-mode responses and lead to a

more uniform envelope of maximum IDRs. As a result, the noticeably enhanced collapse prevention performance was obtained for the structures with R=3.

7 Conclusions and design recommendations

In modular buildings with steel frames, the frame of each module can provide significant lateral resistance as the beams are typically welded to columns. To make use of the inherent lateral resistance in all modules, the distributed seismic design concept is proposed and a capacity-based design method is developed in this study.

To study the seismic behavior of steel modular frames designed following the distributed seismic design method, a numerical parametric study is conducted on a 9-story prototype building. The studied parameters include the rotational stiffness of inter-module connections, the seismic design force level, and the height-wise distribution of the design base shear. The main conclusions are:

(1) For periods associated with modal shapes that involve little rotation of inter-module connections, e.g., the fundamental period, the rotational stiffness of inter-module connections has little impact. For higher modes of vibration which involve large rotation of inter-module connections, increasing rotational stiffness will lead to shorter periods.

(2) If the inter-module connections have no (or little) rotational stiffness (idealized as pinned), the lateral resistance of one module is independent of other modules. In this case, plastic drift tends to concentrate in one module under lateral loading, and a soft-story mechanism is likely to develop with the P-delta effect.

(3) With the increase in the rotational stiffness of inter-module connections, the rotation of columns in one module will be restrained by adjacent modules. As such, the drift concentration in one module will be reduced, and the collapse prevention capacity of steel module frames will be enhanced.

(4) Increasing the level of seismic design force only may not lead to enhanced collapse prevention performance of steel modular frames, as it is also dependent on the height-wise distribution of the design base shear and the response characteristics of the structure.

(5) The effect of different height-wise distributions of the design base shear is dependent on the response characteristics of the structure. When significant higher-mode response is involved in the total response, the Higher-Mode distribution of the design base shear will lead to a more uniform envelope of the maximum IDRs and an enhanced collapse prevention performance. However, in case the seismic response is dominated by the 1st-mode response, the adoption of the Higher-Mode distribution may not have a positive effect on the collapse prevention capacity of steel modular frames.

Based on the findings, the following design recommendations are made:

(1) In design practice, linear analysis is often conducted first to obtain an estimation about the fundamental period of the structure. For such an analysis, engineers may set inter-module connections as either pinned or rigid as the rotational stiffness of inter-module connections has little impact on the fundamental period of modular frame. However, when conducting nonlinear static/dynamic analysis, appropriate rotational stiffnesses that are representative of the adopted inter-module connections shall be defined in the model. The rotational stiffness of the inter-module connections can be evaluated through experimental tests or numerical study.

(2) For design of inter-module connections, in addition to the translational connectivity, sufficient rotational stiffness shall be provided to ensure satisfactory collapse prevention performance. Its sufficiency can be evaluated through NRHAs under a set of ground motion records that are representative of the seismic hazard of the building.

(3) To determine the height-wise distribution of the design base shear, preliminary nonlinear dynamic analyses of the frame under a set of ground motion records are recommended to obtain its response characteristics first. If the total response is dominated by the 1st-mode response, the

552 1st-Mode distribution shall be adopted. Otherwise, if significant higher-mode response is involved,
553 the Higher-Mode distribution shall be adopted.

554 **Limitations**

555 It is worth noting that the findings and conclusions made in this study may be applicable
556 merely to steel modular frames having a similar height to the prototype building and designed
557 following the proposed distributed seismic design method. Moreover, the optimum seismic design
558 force level has not been determined by this study and requires further extensive parametric study
559 which is ongoing by the authors.

560 **Data availability**

561 All data, models, or code that support the findings of this study are available from the
562 corresponding author upon reasonable request.

563 **Acknowledgement**

564 The research work presented in this paper was supported by the Chinese National
565 Engineering Research Centre for Steel Construction (Hong Kong Branch) and the Seed Funding
566 from the Department of Civil and Environmental Engineering at The Hong Kong Polytechnic
567 University. The numerical simulation was conducted on the Higher Performance Computing (HPC)
568 platform at The Hong Kong Polytechnic University. The authors would also like to thank Prof.
569 Liang Zong at Tianjin University for sharing the experimental test data.

570 **References**

571 American Institute of Steel Construction (AISC). (2016). AISC 341-16: Seismic Provisions for Structural Steel
572 Buildings. Chicago, IL: American Institute of Steel Construction.
573 American Institute of Steel Construction (AISC). (2016). AISC 360 -16: Specification for structural steel buildings.
574 Chicago, IL: American Institute of Steel Construction.
575 American Society of Civil Engineers/Structural Engineering Institute (ASCE/SEI) 7-16. (2016). Minimum Design
576 Loads and associated criteria for buildings and other structures. Reston, Virginia, USA.
577 Annan, C. D., Youssef, M. A., & El Naggar, M. H. (2009a). Experimental evaluation of the seismic performance of
578 modular steel-braced frames. *Engineering Structures*, 31(7), 1435-1446.
579 Annan, C. D., Youssef, M. A., & El Naggar, M. H. (2009b). Seismic vulnerability assessment of modular steel
580 buildings. *Journal of Earthquake Engineering*, 13(8), 1065-1088.

CEN. (2004). Eurocode 8: Design of structures for earthquake resistance. Part I: General rules, seismisc actions and rules for buildings. *EN 1998*, European Committee for Standardization, Brussels.

Chao, S. H., Goel, S. C., & Lee, S. S. (2007). A seismic design lateral force distribution based on inelastic state of structures. *Earthquake Spectra*, 23(3), 547-569.

Chen, Z. H., Li, H., Chen, A., Yu, Y., & Wang, H. (2017a). Research on pretensioned modular frame test and simulations. *Engineering Structures*, 151, 774-787.

Chen, Z., Liu, J., Yu, Y., Zhou, C., & Yan, R. (2017b). Experimental study of an innovative modular steel building connection. *Journal of Constructional Steel Research*, 139, 69-82.

Chua, Y. S., Liew, J. R., & Pang, S. D. (2020). Modelling of connections and lateral behavior of high-rise modular steel buildings. *Journal of Constructional Steel Research*, 166, 105901.

Dai, X. M., Zong, L., Ding, Y., & Li, Z. X. (2019). Experimental study on seismic behavior of a novel plug-in self-lock joint for modular steel construction. *Engineering structures*, 181, 143-164.

Dai, Z., Dai Pang, S., & Liew, J. R. (2020). Axial load resistance of grouted sleeve connection for modular construction. *Thin-Walled Structures*, 154, 106883.

Deng, E. F., Zong, L., Ding, Y., & Luo, Y. B. (2018). Seismic behavior and design of cruciform bolted module-to-module connection with various reinforcing details. Thin-Walled Structures, 133, 106-119.

Deng, E. F., Zong, L., Ding, Y., Zhang, Z., Zhang, J. F., Shi, F. W., ... & Gao, S. C. (2020). Seismic performance of mid-to-high rise modular steel construction-A critical review. *Thin-Walled Structures*, 155, 106924.

Fahnestock, L. A., Sause, R., & Ricles, J. M. (2007). Seismic response and performance of buckling-restrained braced frames. *Journal of Structural Engineering*, 133(9), 1195-1204.

Fathieh, A., & Mercan, O. (2016). Seismic evaluation of modular steel buildings. *Engineering Structures*, 122, 83-92.

FEMA. (2009). Quantification of building seismic performance factors. *FEMA P695*, Washington, DC.

Ferdous, W., Bai, Y., Ngo, T. D., Manalo, A., & Mendis, P. (2019). New advancements, challenges and opportunities of multi-storey modular buildings–A state-of-the-art review. *Engineering Structures*, 183, 883-893.

Gatheeshgar, P., Poologanathan, K., Gunalan, S., Shyha, I., Sherlock, P., Rajanayagam, H., & Nagaratnam, B. (2021). Development of affordable steel-framed modular buildings for emergency situations (Covid-19). *Structures* (Vol. 31, pp. 862-875).

He, X.-H.-C., Chan, T.-M. and Chung, K.-F. (2021). "Effect of inter-module connections on progressive collapse behaviour of MiC structures", *Journal of Constructional Steel Research*, Elsevier Science, Vol. 185, 106823.

Hsiao, P. C., Lehman, D. E., & Roeder, C. W. (2013). Evaluation of the response modification coefficient and collapse potential of special concentrically braced frames. *Earthquake engineering & structural dynamics*, 42(10), 1547-1564.

Kamali, M., & Hewage, K. (2016). Life cycle performance of modular buildings: A critical review. *Renewable and sustainable energy reviews*, 62, 1171-1183.

Krawinkler, H., & Seneviratna, G. D. P. K. (1998). Pros and cons of a pushover analysis of seismic performance evaluation. *Engineering structures*, 20(4-6), 452-464.

Lacey, A. W., Chen, W., Hao, H., Bi, K., & Tallowin, F. J. (2019). Shear behaviour of post-tensioned inter-module connection for modular steel buildings. *Journal of Constructional Steel Research*, 162, 105707.

Lawson, R. M., Ogden, R. G., & Bergin, R. (2012). Application of modular construction in high-rise buildings. *Journal of architectural engineering*, 18(2), 148-154.

Lawson, R., & Ogden, R. (2005). Developments in pre-fabricated systems in light steel and modular construction. *Transport*, 35(15), 15.

Liew, J. Y. R., Chua, Y. S., & Dai, Z. (2019, October). Steel concrete composite systems for modular construction of high-rise buildings. *Structures* (Vol. 21, pp. 135-149). Elsevier.

Liu, Y., Chen, Z., Liu, J., Bai, Y., Zhong, X., & Wang, X. (2020). Lateral stiffness evaluation on corner-supported thin walled modular steel structures. *Thin-Walled Structures*, 157, 106967.

M. Lawson, R. Ogden, C. Goodier. (2014). Design in modular construction. *CRC Press*.

MacRae, G. A., Kimura, Y., & Roeder, C. (2004). Effect of column stiffness on braced frame seismic behavior. *Journal of Structural Engineering*, 130(3), 381-391.

Mazzoni, S., McKenna, F., Scott, M. H., and Fenves, G. L. (2009). OpenSees command language manual, Univ. of California, Berkeley, Calif.

McKenna, F. (1997). "Object oriented finite element programming frameworks for analysis, algorithms and parallel computing." Ph.D. dissertation, Univ. of California at Berkeley, CA.

National Research Council of Canada (NRCC). (2015). National Building Code of Canada (NBCC) (13th ed.). Ottawa, ON, Canada.

Smith, R. E. (2010). Prefab architecture: A guide to modular design and construction. *John Wiley & Sons*.

Srisangeerthanan, S., Hashemi, M. J., Rajeev, P., Gad, E., & Fernando, S. (2018). Numerical study on the effects of diaphragm stiffness and strength on the seismic response of multi-story modular buildings. *Engineering Structures*, 163, 25-37.

Wang, C. Tremblay, R. & Rogers, C. A. (2021). Component-based model for bolted brace connections in conventional concentrically braced frames. *Engineering Structures*, Volume 247, 113137.

Xu, F., Wen-Hao Pan, Chan, T.-M., Sheehan, T. and Gardner, L. (2022). "Fracture Prediction for Square Hollow Section Braces under Extremely Low Cycle Fatigue", *Thin-Walled Structures*, Elsevier Science, Vol. 171, 108716.

Appendix A Structural design of the frames with different design parameters

Structure	Story	1	2	3	4	5	6	7	8	9
R6-1st	**Col.**	228.6×177.8×15.9	228.6×177.8×15.9	228.6×177.8×15.9	228.6×127×15.9	228.6×127×15.9	228.6×127×15.9	177.8×177.8×12.7	177.8×177.8×12.7	177.8×177.8×12.7
	F.B.	127×127×7.9	127×127×7.9	127×127×7.9	127×101.6×7.9	127×101.6×7.9	127×101.6×7.9	127×50.8×9.5	101.6×101.6×6.4	101.6×63.5×6.4
	C.B.	127×50.8×9.5	127×50.8×9.5	127×50.8×9.5	127×50.8×9.5	101.6×101.6×6.4	101.6×63.5×6.4	101.6×63.5×6.4	88.9×50.8×6.4	76.2×50.8×4.8
R6-Higher	**Col.**	228.6×228.6×15.9	228.6×177.8×15.9	228.6×177.8×15.9	228.6×177.8×15.9	228.6×177.8×15.9	228.6×127×15.9	228.6×127×15.9	177.8×177.8×12.7	177.8×177.8×12.7
	F.B.	127×127×7.9	127×127×7.9	127×127×7.9	127×127×7.9	127×101.6×7.9	127×101.6×7.9	127×76.2×7.9	127×50.8×9.5	101.6×101.6×6.4
	C.B.	127×50.8×9.5	127×50.8×9.5	127×50.8×9.5	127×50.8×7.9	127×50.8×7.9	101.6×101.6×6.4	101.6×76.2×6.4	101.6×63.5×6.4	101.6×50.8×6.4
R3-1st	**Col.**	254×254×19	254×254×19	254×254×19	228.6×228.6×15.9	228.6×177.8×15.9	228.6×177.8×15.9	228.6×127×15.9	228.6×127×15.9	177.8×177.8×12.7
	F.B.	152.4×127×9.5	152.4×127×9.5	152.4×127×9.5	152.4×127×9.5	152.4×101.6×9.5	152.4×76.2×9.5	127×101.6×7.9	127×76.2×7.9	101.6×76.2×6.4
	C.B.	152.4×127×9.5	152.4×127×9.5	152.4×101.6×9.5	152.4×101.6×9.5	152.4×76.2×9.5	127×127×7.9	127×101.6×7.9	101.6×101.6×6.4	88.9×50.8×6.4
R3-Higher	**Col.**	254×254×19	254×254×19	254×254×19	228.6×228.6×15.9	228.6×177.8×15.9	228.6×177.8×15.9	228.6×177.8×15.9	228.6×127×15.9	228.6×127×15.9
	F.B.	152.4×127×9.5	152.4×127×9.5	152.4×152.4×9.5	152.4×127×9.5	152.4×101.6×9.5	152.4×101.6×9.5	152.4×76.2×9.5	127×101.6×7.9	127×101.6×7.9
	C.B.	152.4×127×9.5	152.4×127×9.5	152.4×101.6×9.5	152.4×101.6×9.5	152.4×101.6×9.5	127×127×7.9	127×101.6×7.9	127×101.6×7.9	101.6×101.6×6.4

Note: Col. = Column; F.B. = Floor beam; C.B. = Ceiling beam; all sections are steel hollow structural sections (HSSs)